A study of nonlocal conductivity in high-temperature superconductors

S. J. Phillipson and M. A. Moore
Department of Physics and Astronomy, University of Manchester, Manchester, M13 9PL, UK.

T. Blum
Department of Physics, University of Virginia, Charlottesville, VA 22901.

(February 7, 2008)

We examine nonlocal conductivity in high-temperature superconductors from a phenomenological point of view. One wants to deduce the properties of the conductivity, especially its inherent length scales, from the transport data. Although this is a challenging *inverse* problem, complicated further by the experimental data not being completely self-consistent, we have made some progress. We find that if a certain form for the conductivity is postulated then one requires positive "viscosity" coefficients to reproduce some of the experimental results. We are able to show that the effects of surfaces on the conductivity are likely to be important and draw comparisons with the treatment of the surface within the hydrodynamic approach put forth by Huse and Majumdar. We also develop an approximation scheme for the conductivity which is more robust than the hydrodynamic one, since it is stable for both positive and negative viscosity coefficients, and discuss the results obtained using it.

PACS numbers: 74.60.-w, 74.25.Fy, 74.60.Ge, 74.20.De

I. INTRODUCTION

The measurement of a substantial nonlocal conductivity in high-temperature superconductors in a magnetic field is thought to imply the existence of moving vortex lines having coherence lengths of the order of the sample thickness, as opposed to pancake vortices readily sliding past one another (for a general review, see Blatter *et al.*[1]). Measurements of nonlocal effects probe the inherent length scales of the problem and thus can be used to investigate issues such as whether the decoupling and melting transitions occur simultaneously[2]. The claims of Safar *et al.*[3] to have observed a sizable nonlocal effect in twinned $YBa_2Cu_3O_{7-\delta}$ (YBCO) are based on two sets of measurements. In the first, which we refer to as the *top* geometry, a current is put into and drawn out of the top of a modified flux transformer while the voltage differences, V_{top} and V_{bot}, are measured (see Fig. 1). In the second, the *side* geometry, the current is withdrawn from the bottom and the voltages, V_{left} and V_{right}, are measured. Safar *et al.*[3] find that the ratios V_{bot}/V_{top} and V_{right}/V_{left} both approach one as they near the melting transition. Taken individually either result might be explained by a local though anisotropic conductivity; but taken together the results are inconsistent with a local description. Safar *et al.*[3] confirm this by analyzing each data set as though the conductivity were local (the Montgomery analysis[4]) and extracting from each the *apparent* conductivity ratio $\sigma^{(a)}_{xx}/\sigma^{(a)}_{zz}$, finding a huge discrepancy in these apparent ratios.

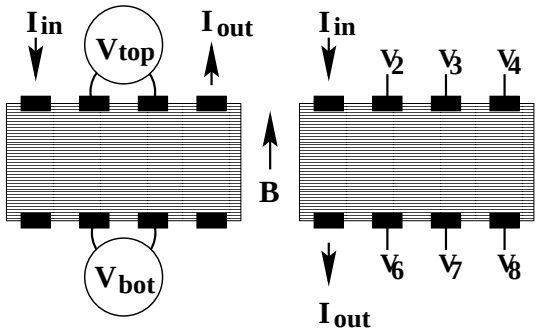

FIG. 1. The modified flux-transformer set-up of Safar *et al.*[3] The diagram on the left shows the arrangement of the terminals for the *top* geometry, and the right shows the *side* geometry. The samples are single crystals of YBCO with the magnetic field aligned along the $\hat{c}$-axis of the crystal. $V_{left} = V_2 - V_6$ and $V_{right} = V_3 - V_7$.

Eltsev and Rapp[5] dispute the Safar *et al.* claim. They performed similar measurements but did not see $V_{right}/V_{left} \to 1$. On the other hand, they may have seen nonlocal effects in a *tilted* geometry in which the current is extracted from terminal 6 (instead of terminal 5) and the ratio $(V_3 - V_8)/(V_2 - V_7)$ measured. In a comparison of twinned and untwinned YBCO, López *et al.*[6] find that in the untwinned YBCO, the strongest signature of nonlocality seen by Safar *et al.*[3], $V_{bot} \approx V_{top}$, is no longer found for any significant temperature range above the "melting" transition. A feature of our studies below is that substantial nonlocal effects are only present when a characteristic length (presumably the phase coherence length) is of the order of the sample thickness. Now the phase coherence length scale along the field direction (ac-

cording to Ref.[7]) grows exponentially rapidly as the temperature is lowered in such a way that the temperature interval over which nonlocal effects might be visible in the vortex-liquid region is only perhaps within $0.3K$ of the temperature at which pinning drives the resistance rapidly to zero. This is of the same order of magnitude as the rounding of the zero-field transition due to sample inhomogeneities and as a consequence it will be hard to disentangle the various effects from each other in the untwinned results of López *et al.*[6]. If one supposes that the long length scale causing the nonlocality in the twinned case is caused by a Bose-glass-like mechanism[8,9], then one would expect the coherence length to increase only as a power law, and the width of the temperature interval over which nonlocal effects are visible may therefore be wider in the twinned case.

The assertions of nonlocal effects in $Bi_2Sr_2CaCu_2O_x$ (BSCCO) are less dramatic than those in YBCO. In their measurements on single-crystal BSCCO, Keener *et al.*[10] never observe the ratios V_{bot}/V_{top} and V_{right}/V_{left} simultaneously approaching one. Nevertheless, when they perform a Montgomery analysis on their data, they do see discrepancies in the apparent ratio $\sigma_{xx}^{(a)}/\sigma_{zz}^{(a)}$. Conversely, measurements by Busch *et al.*[11] on single-crystal BSCCO and by Doyle *et al.*[12] on BSCCO with columnar defects are claimed to be consistent with local resistivity. These seemingly contradictory results could be caused by approximations used in the local analysis[11] and might be resolved by using the full analysis or better suited approximations, such as the one proposed by Levin[13]. A theoretical framework which could provide some quantitative analysis of these results—for example, by the extraction of a temperature-dependent length scale—would obviously be helpful in the interpretation of these and other results. Our aim is to develop such a framework. We will approach the problem phenomenologically, attempting to relate the current-voltage characteristics to the form of the (nonlocal) conductivity.

When a material has a nonlocal conductivity, the appropriate form of Ohm's law is given by

$$j_\mu(\mathbf{r}) = \int \sigma_{\mu\nu}(\mathbf{r},\mathbf{r}')\, E_\nu(\mathbf{r}')\, d^3r', \tag{1}$$

where symbols have their usual meaning in this context, and the integral is taken over the volume of the sample. For a nonlocal conductivity, $\sigma_{\mu\nu}(\mathbf{r},\mathbf{r}') \neq \sigma_{\mu\nu}\,\delta(\mathbf{r}-\mathbf{r}')$. In momentum space, for a translationally invariant system, this relation becomes

$$\hat{\jmath}_\mu(\mathbf{k}) = \hat{\sigma}_{\mu\nu}(\mathbf{k})\,\hat{E}_\nu(\mathbf{k}), \tag{2}$$

where $\hat{\jmath}_\mu(\mathbf{k})$ is the Fourier transform of $j_\mu(\mathbf{r})$, and similarly for the other quantities. It should be noted that nonlocal effects will only be observable when the length scale of the nonlocality is of the same order or larger than the distance between leads.

The best known theoretical work on the subject is the "hydrodynamic" approach, expounded upon in general by Marchetti *et al.*[14] and applied specifically to the conductivity by Huse and Majumdar[15]. This theory is so-called because the nonlocal conductivity $\hat{\sigma}_{\mu\nu}(\mathbf{k})$ is expanded in a Taylor series in $\mathbf{k}$, and the expansion is terminated at order k^2; in other words, the conductivity is taken to be of the form

$$\hat{\sigma}_{\mu\nu}(\mathbf{k}) = \hat{\sigma}_{\mu\nu}(\mathbf{0}) + \eta_{\mu\beta\gamma\nu}\, k_\beta k_\gamma. \tag{3}$$

We revert to the notation of Huse and Majumdar to facilitate comparison with that work[15]; note that later works[16–18] replace the η's with S's to prevent confusion with the viscosity tensor of the vortex-line liquid, which is related but distinct[16]. Unfortunately, this form for the conductivity is unphysical if certain coefficients become negative, as shown by Blum and Moore[17]. Huse and Majumdar always assume that the coefficients they use are positive. When and whether the coefficients are in fact positive or negative will be discussed in more detail in Section II.

The hydrodynamic analysis leads to a fourth-order partial differential equation which reduces to Laplace's equation in the local limit ($\eta = 0$). It also supplies sufficient boundary conditions to solve for the potential $V(\mathbf{r})$. Huse and Majumdar argue that there are discontinuities in the first derivative of $\mathbf{E}(\mathbf{r})$ at the surface. When the conductivity (which in hydrodynamics is a differential operator) is applied, the result is δ-functions in the current distribution at the surface, i.e. surface currents. One then uses charge conservation, $\nabla\cdot\mathbf{j} = 0$, to translate this outcome into boundary conditions on $V(\mathbf{r})$. To handle the δ-function it is convenient to integrate over the surface as in the standard Gaussian pillbox arguments[19]—only here, because of the surface current, the side surfaces of the pillbox contribute even as the volume of the box is shrunk down to zero. This gives what initially looks like an extra term in their boundary conditions.

Huse and Majumdar study a two-dimensional geometry modeling the flux transformer used in the experiments, the z-axis of which coincides with the $\hat{c}$-axis of the superconductor. They have performed a detailed analysis of the situation with one non-zero viscosity coefficient, η_{xzzx}, which embodies the interaction of pancake vortices moving in different ab planes and at different velocities. Somewhat surprisingly, their equation and boundary conditions are symmetric under $\eta_{xzzx} \leftrightarrow \eta_{zxxz}$ despite the fact that these coefficients would appear to represent very different physics.

As an alterative to the hydrodynamic truncation of $\hat{\sigma}_{\mu\nu}(\mathbf{k})$, we consider an analysis based on Padé approximations to $\hat{\sigma}_{\mu\nu}(\mathbf{k})$. It incorporates a more realistic large-$\mathbf{k}$ behavior than the hydrodynamic approach and remains solvable. In principle, one can approximate $\hat{\sigma}_{\mu\nu}(\mathbf{k})$ to any desired degree of accuracy by using a sufficiently large-order Padé approximation. As the order of the approximation is increased, our technique of solution continues to work, but the computing effort increases rapidly. One

stage of the solution involves a partial differential equation rather reminiscent of that occurring in hydrodynamics. In fact, in one instance we can recover the results of Huse and Majumdar by means of a limiting procedure on the Padé result.

In the remainder of this paper we first discuss our motivation for wanting to improve upon and extend the work of Huse and Majumdar; this involves an examination of whether the relevant coefficients η in the small-k expansion of the conductivity are positive or negative. We investigate the current-voltage characteristics in a particular geometry (the infinite-slab geometry), which allows us to comment on whether positive or negative viscosity coefficients are needed to explain experimental data like that of Safar *et al.*[3] (Sec. III). The section following that contains details of work using Padé approximations to the conductivity. In Sec. V we discuss the role of surfaces in determining the conductivity and how the analysis of Huse and Majumdar takes account of surfaces. Appendices A and B contain some calculational details, while in Appendix C we outline the Bose-glass scaling of the conductivities used in some of the numerical work.

II. ARE THE VISCOSITY COEFFICIENTS NEGATIVE OR POSITIVE?

For stability, the conductivity tensor $\hat{\sigma}_{\mu\nu}(\mathbf{k})$ must be a positive definite matrix. For this to be true of the hydrodynamic form, Eq. (3), certain of the viscosity coefficients $\eta_{\mu\alpha\beta\nu}$ must be positive; in particular, η_{zzzz} and η_{xxxx}. The work of Mou *et al.*[16] and Blum and Moore[17] shows that for high temperatures, these coefficients are actually negative. Both works use the time-dependent Ginzburg-Landau equation as a starting point, so "high temperatures" in this context means near the $H_{c2}(T)$ line. Thus to treat nonlocal conductivities in this region of the H-T plane, one requires a model that can handle these so-called negative viscosities, ruling out the hydrodynamics approach. However, we expect substantial nonlocal behavior occurs only near the melting line, where some of the viscosities may very well be positive and hydrodynamics a viable approach.

So what happens to $\hat{\sigma}_{\mu\nu}(\mathbf{k})$ as the temperature is lowered? The arguments of Mou *et al.*[16] suggest and the simulations of Wortis and Huse[18] bear out that as the temperature is decreased, η_{xxxx} changes sign, becoming positive. Imagine a plot of $\hat{\sigma}_{xx}(k_x)$ (see Wortis and Huse[18]): at high temperatures, $\hat{\sigma}_{xx}(k_x)$ increases monotonically as k_x is decreased, but at low temperatures, it develops a local maximum at a nonzero k_x and then falls to a finite value (the flux-flow value[20]) at $k_x = 0$.

In the presence of a magnetic field, the ab-plane conductivity of a type-II superconductor does not diverge, because a current causes the vortices to move, leading to dissipation, that is, a non-zero resistance. The conductivity is thus enhanced if this movement of vortices is impeded, for instance by pinning centers. The interaction of a vortex with other vortices may also inhibit its motion. However, for a uniform current the vortices all move together and thus their mutual interactions play little role in hindering the center-of-mass motion. For a nonuniform current, on the contrary, the vortices are impelled to change their relative positions, and so their interactions do inhibit this sort of motion. Therefore, the conductivity may be higher for a nonuniform current. These arguments suggest that at low temperatures where the interactions become important the conductivity might be higher at some nonzero k_x.

The situation is different for conductivity along the $\hat{c}$-axis. Like $\hat{\sigma}_{xx}(k_x)$, at high temperatures, $\hat{\sigma}_{zz}(k_z)$ increases monotonically as k_z is lowered. However, the current is now along the axis of the vortices, the vortices are not forced to move, and this time the uniform conductivity $\hat{\sigma}_{zz}(\mathbf{k} = \mathbf{0})$ diverges as the temperature is lowered. Hence, there is no compelling reason to expect that a local maximum will develop as temperature is lowered, and one might suspect that η_{zzzz} remains negative and therefore unsuited for the hydrodynamic prescription at all temperatures. This expectation for η_{zzzz} seems to be borne out by low-temperature calculations which have the Abrikosov lattice as a starting point[21] and also by the preliminary simulation results[22].

The proposition that some of the η's may be negative at all temperatures is one motive for wanting an alternative to hydrodynamics; there are others. Hydrodynamics is a simple approximation to the actual conductivities, but we do not know how good an approximation it is. Plus, there is no obvious way to improve upon it—one might include terms of order k^4, but this necessitates additional boundary conditions to specify the solution, and it is unclear what they would be. In the Fourier representation of a function, the small-k terms model well its bulk properties, but higher-k terms are needed to capture the behavior at the boundaries. So one might think a procedure focusing on small-k would do well in the bulk and perhaps less satisfactorily at the surface. But hydrodynamics involves a differential equation, and its solution, even in the bulk, is determined by boundary conditions, i.e. the surface. Thus it is crucial to treat the surface properly—even more so, since in the experiments at issue here, all of the measurements are taken at the surface. Huse and Majumdar do take some account of surfaces, and in doing so find surface currents, but their theory is unable to make any prediction about the length scale over which these currents might flow. Such restrictions as these provide the impetus to go beyond hydrodynamics.

There is one further comment that is useful to make before proceeding to some concrete calculations. While we require that $\hat{\sigma}_{\mu\nu}(\mathbf{k})$ be a positive definite matrix, this does not imply that $\sigma_{\mu\nu}(\mathbf{r})$ must always be positive. Although conductivities taking on negative values seems a little odd at first sight, the simulations of Wortis and Huse[18] find that $\sigma_{xx}(x, k_y = 0)$ can be negative over a range of a few inter-vortex spacings. In fact, *any* non-

locality in the conductivity implies that either the real-space conductivity or resistivity (or both) take on negative values at some points. By definition, the conductivity matrix is the inverse of the resistivity matrix, which implies that in Fourier space, $\hat{\sigma}_{\mu\nu}(\mathbf{k})\hat{\rho}_{\nu\alpha}(\mathbf{k}) = \delta_{\mu\alpha}$ ($\delta_{\mu\alpha}$ is the Kronecker delta function and the summation convention is used). For example, if $\sigma_{xy} = \sigma_{xz} = 0$ we have in real space

$$\int d^3r'\, \sigma_{xx}(\mathbf{r} - \mathbf{r}')\, \rho_{xx}(\mathbf{r}' - \mathbf{r}'') = \delta(\mathbf{r} - \mathbf{r}''). \qquad (4)$$

If $\mathbf{r} \neq \mathbf{r}''$, the right hand side of Eq. (4) is zero; for the left hand side to be zero, some cancellation is needed. However, there would be no cancellation if $\sigma_{xx}(\mathbf{r} - \mathbf{r}')$ and $\rho_{xx}(\mathbf{r}' - \mathbf{r}'')$ are both everywhere positive. Thus, one or both has negative regions. For experimental setups in which the current is distributed throughout the sample, this feature may not manifest itself in the voltage distribution; thus, Wortis and Huse [18] have proposed geometries with very localized currents in order to look for it.

III. THE INFINITE-SLAB GEOMETRY AND POSITIVE VISCOSITIES

The aim of this section is to show that for the choice of conductivity given below, it is necessary to have *positive* viscosity coefficients to produce the strongly nonlocal behavior seen by Safar *et al.*[3]: $V_{bot}/V_{top} \to 1$ and $V_{right}/V_{left} \to 1$ simultaneously. Let us consider the two-dimensional geometry shown in Fig. 2, with the lateral dimension $L \to \infty$; taking this limit eliminates one set of boundary effects. Furthermore, let us postulate conductivities of the form

$$\hat{\sigma}_{xx}(\mathbf{k}) = \Sigma_x; \qquad (5a)$$
$$\hat{\sigma}_{zz}(\mathbf{k}) = \hat{\sigma}_{zz}(k_x), \qquad (5b)$$

that is, $\hat{\sigma}_{xx}$ is a constant (i.e. local) and $\hat{\sigma}_{zz}$ is a function of k_x alone. The function $\hat{\sigma}_{zz}(k_x)$ may include a constant piece; moreover, that constant, as well as Σ_x, may represent both superconducting and normal contributions to the local conductivity. Restricting the wavevector dependence to k_x alone enables us to solve for the potential $V(x, z)$ via Fourier transformation.

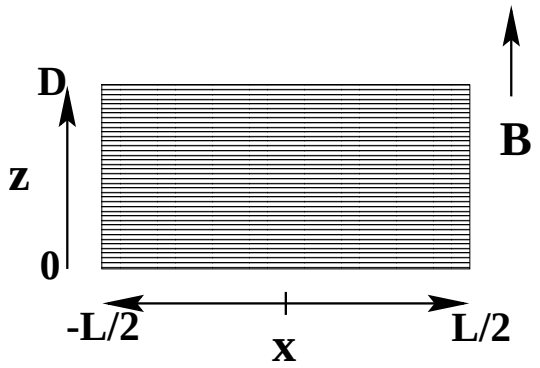

FIG. 2. The geometry used for our calculations of the potential $V(x, z)$. The $\hat{c}$-axis of the superconductor is aligned along the z-axis (called the y-axis in the notation of Huse and Majumdar).

To determine $V(x, z)$ for a given input current, first relate $V(x, z)$ to the components of the current

$$j_x(x, z) = -\Sigma_x\, \partial_x V(x, z); \qquad (6a)$$
$$j_z(x, z) = -\int_{-\infty}^{\infty} \sigma_{zz}(x - x')\, \partial_z V(x', z)\, dx', \qquad (6b)$$

using $E_\mu = -\partial_\mu V$. Next note that in the steady state, the continuity equation is $\boldsymbol{\nabla} \cdot \mathbf{j} = 0$, which in this case is

$$\Sigma_x\, \partial_x^2 V(x, z) + \int_{-\infty}^{\infty} \sigma_{zz}(x - x')\, \partial_z^2 V(x', z)\, dx' = 0. \qquad (7)$$

Fourier transforming Eq. (7) with respect to x yields

$$-\Sigma_x\, k_x^2\, \hat{V}(k_x, z) + \hat{\sigma}_{zz}(k_x)\, \partial_z^2 \hat{V}(k_x, z) = 0, \qquad (8)$$

where we have used the fact that the transform of the convolution is the product of the transforms. The solution of this differential equation is

$$\hat{V}(k_x, z) = A(k_x) \cosh[\kappa(k_x) z] + B(k_x) \sinh[\kappa(k_x) z], \quad (9)$$

where

$$\kappa^2(k_x) = \frac{\Sigma_x\, k_x^2}{\hat{\sigma}_{zz}(k_x)}. \qquad (10)$$

One determines the functions $A(k_x)$ and $B(k_x)$ from the boundary conditions; toward this end, it is convenient to Fourier transform the expression for j_z (Eq. (6b))

$$\hat{\sigma}_{zz}(k_x)\, \partial_z \hat{V}(k_x, z) = -\hat{j}_z(k_x, z). \qquad (11)$$

Imposing the boundary conditions appropriate for the top geometry, namely $j_z(x, 0) = 0$ and $j_z(x, D) = J_T(x)$, finding $\hat{V}(k_x, z)$ and taking the inverse transform yields

$$V_T(x, z) = -\int_{-\infty}^{\infty} \frac{dk_x}{2\pi} \frac{\hat{J}_T(k_x) \cosh(\kappa z)\, \mathrm{e}^{ik_x x}}{\kappa\, \hat{\sigma}_{zz}(k_x)\, \sinh(\kappa D)}. \qquad (12)$$

Note that charge conservation implies $\hat{J}_T(0) = 0$, and hence the integral above converges at $k_x = 0$. For the side geometry, similar manipulations using the boundary conditions $j_z(x,0) = j_z(x,D) = J_S(x)$ give

$$V_S(x,z) = \int_{-\infty}^{\infty} \frac{dk_x}{2\pi} \frac{\hat{J}_S(k_x) \sinh\left[\kappa\left(\frac{D}{2} - z\right)\right] e^{ik_x x}}{\kappa\, \hat{\sigma}_{zz}(k_x)\, \cosh\left(\frac{\kappa D}{2}\right)}. \quad (13)$$

Analytically the x-axis decay length is controlled by the pole structure of the above integrals (see Appendix A for more details). Rather generically, this length grows if the viscosity coefficient (the coefficient of k_x^2 in the small-k_x expansion of $\sigma_{zz}(k_x)$) is positive, leading to features such as $V_{right}/V_{left} \to 1$. Increasing this coefficient (η) also changes the ratio V_{bot}/V_{top} though not necessarily in a monotonic fashion. However, there is another way to ensure that $V_{bot}/V_{top} \to 1$: this is simply to make σ_{zz} very large, which applies even in the local limit. Thus, to obtain results like those of Safar *et al.* [3], we expect that a $\hat{\sigma}_{zz}(k_x)$ which grows large and has a positive viscosity coefficient at low temperatures is required.

These arguments have been checked numerically for a variety of conductivities. One example is shown in Fig. 3. We have put all of the temperature dependence of the conductivity into the length scale ℓ which is presumed to increase as temperature decreases and choose a conductivity of the form $\hat{\sigma}_{zz}(k_x) = \sigma_z^{(n)} + C\ell^2(1 + 2k_x^2\ell^2)/(1 + k_x^2\ell^2)$, which meets the above criterion as ℓ increases. Note that we have also included $\sigma_z^{(n)}$, a local term that does *not* scale with ℓ. Fig. 3 shows a plot of V_{bot}/V_{top} and V_{right}/V_{left} as a function of $1/\ell$, for this choice. It can be seen that as $\ell \to \infty$, the two ratios do indeed approach one.

Using conductivities with negative viscosity gives results such as those shown in Figs. 4 and 5. In this particular case, the conductivity used was $\hat{\sigma}_{zz}(k_x) = \sigma_z^{(n)} + C\ell e^{-k_x^2\ell^2}$; however, the results are typical of conductivities with negative viscosity. Finding negative voltages is not necessarily unphysical (see the discussion surrounding Eq. (4)) but the results clearly do not give us the strongly nonlocal behavior seen by Safar *et al.* [3].

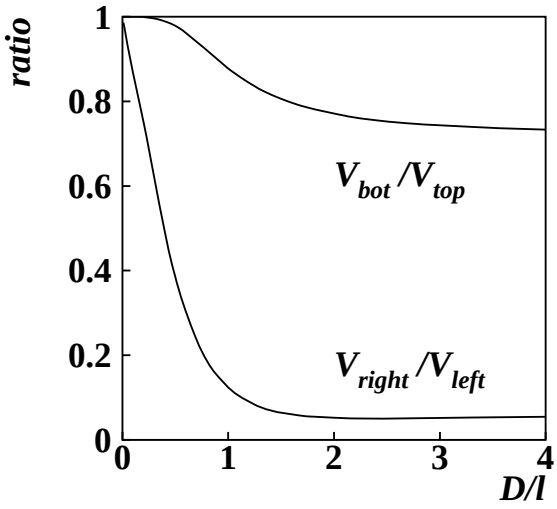

FIG. 3. The ratios of V_{bot}/V_{top} and V_{right}/V_{left} for the conductivity with positive viscosity coefficients, the form of which is provided in the text. The boundary conditions used were $J_T(x) = J_0\,[\delta(x - 2L_c) - \delta(x + 2L_c)]$ and $J_S(x) = -J_0\,\delta(x + 2L_c)$ ($4L_c$ is defined to be the distance between the current inputs). The voltages V_{top} and V_{bot} were measured at $x = \pm L_c$ as were the voltages V_2, V_3, V_6 and V_7. The parameters used are $\Sigma_x = 5$, $\sigma_z^{(n)} = 1$, $C = 1$, $D = 1$ and $L_c = 1$; this corresponds to measuring lengths in terms of the thickness of the sample and conductivities in terms of $\sigma_z^{(n)}$, as will also be done in all the other figures.

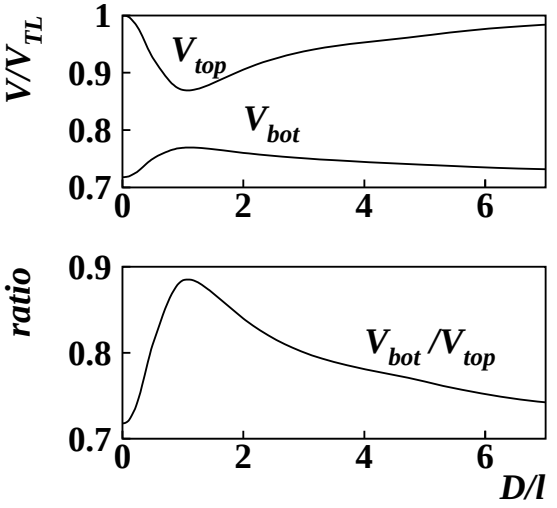

FIG. 4. The voltages V_{top} and V_{bot} and their ratio for the conductivity $\hat{\sigma}_{zz}(k_x) = \sigma_z^{(n)} + C\ell e^{-k_x^2\ell^2}$, with the same values of parameters as in Fig. 3. By definition, V_{TL} is defined to be V_{top} in the local case for this geometry, which can be calculated from Eq. (A2). Note that V_{bot}/V_{top} does not tend to 1 as $\ell \to \infty$.

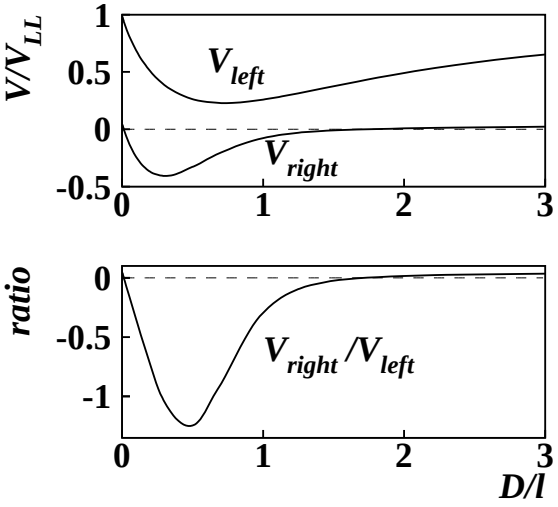

FIG. 5. The voltages V_{left} and V_{right} and their ratio for the conductivity $\hat{\sigma}_{zz}(k_x) = \sigma_z^{(n)} + C\ell e^{-k_x^2\ell^2}$, with the same parameters as for Figs. 3 and 4. Here, V_{LL} is defined to be V_{left} for the local case, Eq. (A2). The notable feature here is that V_{right} becomes negative.

Now let us consider the difference between the experimental data taken from twinned YBCO[3] and untwinned YBCO[6]. Recall that for the twinned YBCO, the V_{top} and V_{bot} curves meet at some temperature T_{th}, and they continue toward zero together as the temperature is lowered. For the untwinned YBCO, on the other hand, the curves only meet just before dropping sharply to zero. We can reproduce some of these features by choosing the scaling forms for the conductivity appropriately, depending upon whether the sample is twinned or untwinned. For the twinned case, we use the Bose-glass scaling forms, which are discussed in Appendix C. Although these are supposed to be valid in the presence of columnar defects, and not strictly twin planes, we use them here since there is currently no better alternative, and there is at least some experimental evidence[23] to support a Bose-glass transition in twinned YBCO. For the untwinned case, we will use the same forms used to generate Fig. 3.

We choose conductivities given by

$$\begin{aligned} &\text{Untwinned:} \quad \begin{cases} \hat{\sigma}_{xx} = \sigma_x^{(n)} \\ \hat{\sigma}_{zz} = \sigma_z^{(n)} + \dfrac{C_1\ell^2\left(1+2k_x^2\ell^2\right)}{1+k_x^2\ell^2}, \end{cases} \\ &\text{Twinned:} \quad \begin{cases} \hat{\sigma}_{xx} = \sigma_x^{(n)} + C_2\ell^4 \\ \hat{\sigma}_{zz} = \sigma_z^{(n)} + \dfrac{C_1\ell^6\left(1+2k_x^2\ell^2\right)}{1+k_x^2\ell^2}. \end{cases} \end{aligned} \tag{14}$$

Both choices have the same overall form with positive viscosity coefficients, the only difference is in how the constants scale with ℓ.

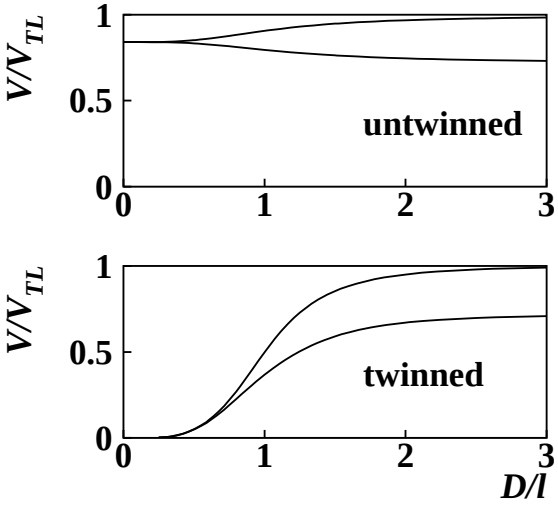

FIG. 6. The results for V_{top} and V_{bot} as a function of ℓ, using the conductivities of Eq. (14) with parameters $\sigma_x^{(n)} = 5$, $\sigma_z^{(n)} = 1$, $D = 1$, $C_1 = 1$ and $C_2 = 5$. The upper curve in each plot is V_{top}, and the lower is V_{bot}.

The results obtained are shown in Fig. 6. Firstly, it can be seen that in both instances, $V_{top}/V_{bot} \to 1$ as the length scale ℓ is increased. However, for the twinned case, both V_{top} and V_{bot} tend to zero together, whereas in the untwinned case, they tend to some finite value. If one identifies the sharp drop in the corresponding experimental results as the transition from a vortex liquid to solid, then this is the correct behavior. The voltages in Fig. 6 level off as ℓ grows small, whereas the voltages measured in the experiments continue to rise as the temperature is increased. This discrepancy is due to our neglect of, among other things, the temperature dependence of the normal component, which can be nontrivial[24]. Nevertheless, the results show that varying the scaling behavior can account for some of the differences between the twinned and untwinned YBCO.

IV. WORK WITH PADÉ APPROXIMATIONS

In this section, we lift some of the restrictions in the previous section by considering a flux-transformer geometry with finite lateral dimension L and by generalizing the nonlocal conductivities of Eq. (5) to allow either $\hat{\sigma}_{xx}$ or $\hat{\sigma}_{zz}$ to be nonlocal and depend on either k_x or k_z. As opposed to the infinite-slab geometry, we could not make progress with general conductivities, thus we elect to use Padé approximations to the conductivities. Two important advantages to using Padé forms are: 1) they capture the high-$\mathbf{k}$ behavior as well as the low-$\mathbf{k}$ behavior of the true conductivity and 2) the resulting equations are analytically soluble. In addition, the corresponding real-space conductivities can be chosen to be decaying exponentials, which, according to Wortis and Huse[18], could

be the correct form for the high-temperature regime.

We will consider four different cases:

$$1.\ \hat{\sigma}_{xx}(\mathbf{k}) = \Sigma_x, \quad \hat{\sigma}_{zz}(\mathbf{k}) = \Sigma_z + \frac{\Delta_z^z}{1+k_z^2\ell^2}; \tag{15a}$$

$$2.\ \hat{\sigma}_{zz}(\mathbf{k}) = \Sigma_z, \quad \hat{\sigma}_{xx}(\mathbf{k}) = \Sigma_x + \frac{\Delta_x^z}{1+k_z^2\ell^2}; \tag{15b}$$

$$3.\ \hat{\sigma}_{zz}(\mathbf{k}) = \Sigma_z, \quad \hat{\sigma}_{xx}(\mathbf{k}) = \Sigma_x + \frac{\Delta_x^x}{1+k_x^2\ell^2}; \tag{15c}$$

$$4.\ \hat{\sigma}_{xx}(\mathbf{k}) = \Sigma_x, \quad \hat{\sigma}_{zz}(\mathbf{k}) = \Sigma_z + \frac{\Delta_z^x}{1+k_x^2\ell^2}. \tag{15d}$$

Note that the momentum dependence is upon k_z in Cases 1 and 2 whereas it is upon k_x in Cases 3 and 4 and that $\hat{\sigma}_{xx}$ is local in Cases 1 and 4 while $\hat{\sigma}_{zz}$ is local is Cases 2 and 3. In the Padé form, Σ is the conductivity as $k \to \infty$, $\Sigma + \Delta$ is that at $k = 0$, and ℓ is a length scale. We set out to solve $\boldsymbol{\nabla} \cdot \mathbf{j} = 0$ subject to the usual boundary conditions on the current at the surface. Each of these problems involves an integro-differential equation, which can be converted into a partial differential equation with linear coefficients, which can in turn be solved by separation of variables. This procedure is outlined in Appendix B. Below we point out some of the distinguishing features of the various cases.

Case 1. With conductivities of the form in Eq. (15a), solving $\boldsymbol{\nabla} \cdot \mathbf{j} = 0$ leads to the partial differential equation

$$\left[\partial_z^4 + \frac{\Sigma_x}{\Sigma_z}\partial_z^2\partial_x^2 - \frac{(1+\gamma_z^z)}{\ell^2}\partial_z^2 - \frac{\Sigma_x}{\Sigma_z\ell^2}\partial_x^2\right] V = 0, \tag{16}$$

where γ_μ^ν is a dimensionless variable given by $\gamma_\mu^\nu = \Delta_\mu^\nu/\Sigma_\mu$. Separation of variables, $V(x,z) = X(x)\,Z(z)$, then yields

$$\left(\frac{d^2}{dx^2} + k^2\right) X = 0, \tag{17a}$$

$$\left\{\frac{d^4}{dz^4} - \left[\frac{\Sigma_x k^2}{\Sigma_z} + \frac{(1+\gamma_z^z)}{\ell^2}\right]\frac{d^2}{dz^2} + \frac{\Sigma_x k^2}{\Sigma_z\ell^2}\right\} Z = 0. \tag{17b}$$

The solution of Eq. (17a) is $X(x) = A\cos(kx) + B\sin(kx)$. Applying the boundary condition that no current enters on the sides, i.e. $\partial_x V(\pm L/2, z) = 0$, gives $k = n\pi/L$ with $B = 0$ for even n and $A = 0$ for odd n. When $n > 0$, the solution of Eq. (17b) is

$$Z(z) = A\mathrm{e}^{z/\xi_+} + B\mathrm{e}^{-z/\xi_+} + C\mathrm{e}^{z/\xi_-} + E\mathrm{e}^{-z/\xi_-}, \tag{18}$$

which has two length scales given by

$$\xi_\pm^{-2}(n) = \frac{1}{2}\left\{\frac{n^2}{\lambda_z^2} + \frac{1+\gamma_z^z}{\ell^2} \pm \left[\left(\frac{n^2}{\lambda_z^2} + \frac{1+\gamma_z^z}{\ell^2}\right)^2 - \frac{4n^2}{\ell^2\lambda_z^2}\right]^{1/2}\right\}, \tag{19}$$

where $\lambda_z = \sqrt{\Sigma_z L^2/\pi^2\Sigma_x}$ is a length scale occurring in the local limit ($\gamma_z^z = 0$). Note that if $\gamma_z^z > 0$ (corresponding to a negative viscosity coefficient) the ξ's are real; whereas if $\gamma_z^z < 0$ (corresponding to a positive viscosity coefficient) the ξ's can become complex.

Case 2. For conductivities given by Eq. (15b), the corresponding differential equation is

$$\left[\partial_z^4 + \frac{\Sigma_x}{\Sigma_z}\partial_z^2\partial_x^2 - \frac{1}{\ell^2}\partial_z^2 - \frac{\Sigma_x}{\Sigma_z}\frac{(1+\gamma_x^z)}{\ell^2}\partial_x^2\right] V = 0. \tag{20}$$

Proceeding with separation of variables, the functions $X_n(x)$ are exactly the same as in Case 1, and the functions $Z_n(z)$ have the same form as in Eq. (18), but the two length scales $\xi_\pm$ are now given by

$$\xi_\pm^{-2} = \frac{1}{2}\left\{\frac{n^2}{\lambda_z^2} + \frac{1}{\ell^2} \pm \left[\left(\frac{n^2}{\lambda_z^2} - \frac{1}{\ell^2}\right)^2 - \frac{4n^2\gamma_x^z}{\ell^2\lambda_z^2}\right]^{1/2}\right\}. \tag{21}$$

As opposed to Case 1, this time when $\gamma_x^z < 0$ the ξ's are real; and when $\gamma_x^z > 0$ the ξ's may become complex.

Case 3. Turning the example with conductivities given by Eq. (15c) into a partial differential equation yields

$$\left[\partial_x^4 + \frac{\Sigma_z}{\Sigma_x}\partial_x^2\partial_z^2 - \frac{(1+\gamma_x^x)}{\ell^2}\partial_x^2 - \frac{\Sigma_z}{\Sigma_x\ell^2}\partial_z^2\right] V = 0. \tag{22}$$

And separation of variables leads to

$$\left\{\frac{d^4}{dx^4} + \left[\frac{\Sigma_z\kappa^2}{\Sigma_x} - \frac{(1+\gamma_x^x)}{\ell^2}\right]\frac{d^2}{dx^2} - \frac{\Sigma_z\kappa^2}{\Sigma_x\ell^2}\right\} X = 0; \tag{23a}$$

$$\left(\frac{d^2}{dz^2} - \kappa^2\right) Z = 0. \tag{23b}$$

We see here that this situation differs from the previous two in that the solution of $X(x)$ is no longer simply sines and cosines, and similarly κ has become nontrivial. This feature complicates the application of the boundary conditions and the summing over eigenfunctions necessary to achieve a complete solution.

Case 4. Conductivities of the form Eq. (15d) lead to

$$\left[\partial_x^4 + \frac{\Sigma_z}{\Sigma_x}\partial_x^2\partial_z^2 - \frac{1}{\ell^2}\partial_x^2 - \frac{\Sigma_z}{\Sigma_x}\frac{(1+\gamma_z^x)}{\ell^2}\partial_z^2\right] V = 0. \tag{24}$$

The method of solution is like that for Case 3, including the nontrivial values of κ.

Results. Let us now consider the results of using Padé approximants. We look at the behavior of V_{top} and V_{bot} as a function of ℓ, as in the previous section. In Cases 1 and 2, we input a current

$$I_{top}(x) = I_1\sin(\pi x/L); \quad I_{bot}(x) = 0 \tag{25}$$

for the top geometry, and

$$I_{top}(x) = I_{bot}(x) = I_0\left[1 + \sin(\pi x/L)\right] \tag{26}$$

for the side geometry. These currents are chosen because they roughly approximate the experimental inputs but involve the minimum number of Fourier components, which simplifies the calculation. If we input the same currents in Cases 3 and 4, our solution will involve an infinite number of terms since our formula for $V(x,z)$ is not in the form of a Fourier series but is a sum over more complicated eigenfunctions. We instead expand the current in terms of these eigenfunctions. In fact, we once again choose the input currents that minimize the number of terms in the sum over eigenfunctions. In the top geometry, the current is chosen to be proportional to the eigenfunction corresponding to κ_1, where κ_1 is the eigenvalue which tends to π/L in the local limit. For the side geometry, we choose the combination of two eigenfunctions that tends to the current of Eq. (26). For Case 3, this unfortunately means that we vary the input current as we vary ℓ; at $\ell = 0$, the input current is the same as for Cases 1 and 2, but this smoothly evolves so that in the limit of $\ell \to \infty$, the input current is $I_{top} \approx I_2 \sin(2\pi x/L)$. The side geometry is affected similarly. Hence, we must bear in mind that the input current changes significantly in Case 3. In Case 4, on the contrary, the variation of input current with ℓ does not appear to be as substantial. The voltages were calculated at $z = 0$, $z = D$ and $x = \pm 0.3L$. For each case, we did two sets of calculations: one using the conductivities as written in Eqs. (15) with Δ scaling as ℓ^2, and the second using the scaling forms appropriate for a Bose glass; as given in Appendix C by Eqs. (C3a)—(C3d).

The first point to make about all of the results is that we never found $V_{right}/V_{left} \to 1$ so long as $\Delta > 0$, which corresponds to a negative viscosity coefficient. Hence none of these forms give us the strongly nonlocal behavior seen by Safar *et al.*[3] (though perhaps they do resemble other results[5,10]). We showed in the infinite-slab case (Sec. III), in which the conductivities corresponded most closely to Case 4, that we could only model Safar's results with positive viscosity coefficients. The results of this section suggest that this statement may hold for all of the cases.

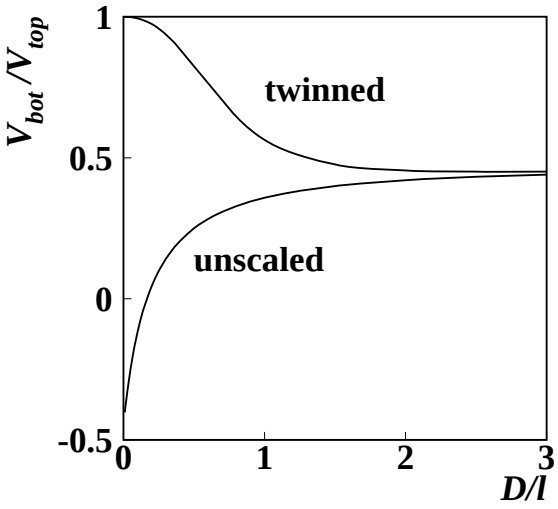

FIG. 7. The results obtained for the ratio V_{bot}/V_{top} for Case 2. The conductivities used are given by Eq. (15b) for the lower curve, and Eq. (C3b) for the upper curve (which has the appropriate scaling for a twinned sample). The parameters used are $\Sigma_x = \sigma_x^{(n)} = 5$, $\Sigma_z = \sigma_z^{(n)} = 1$, $\ell_\parallel \equiv \ell$, $D = 1$, $L = 5$, $C_1 = 1$, $C_2 = 5$ and $\Delta_x^z = 5\ell^2$ — note the scaling with ℓ which is present. For the twinned case, V_{bot}/V_{top} does in fact tend to 1 as $\ell \to \infty$.

Secondly, we look at the difference between the Bose-glass scaled and unscaled results. We have already seen one example of this comparison in Fig. 6. Another appears in Fig. 7, this time for Case 2. The curves are remarkably different considering they came from the same overall form of the conductivity, Eqs. (15b), which shows how vastly different behaviors can be modeled by the same form, making it difficult to extract detailed information on the conductivity from the experimental data.

Recall that the analysis of Huse and Majumdar[15], discussed in the introduction, has a symmetry under $\eta_{xzzx} \leftrightarrow \eta_{zxxz}$. If this symmetry applies in the Padé analysis, it would correspond to a symmetry between Cases 2 and 4. We have looked for such a symmetry. The comparison is complicated by the fact that the eigenfunctions $X_n(x)$ are different in the two cases, as mentioned above. However, using conductivities given by Eq. (15) led to qualitatively different features for Cases 2 and 4—while admittedly the Case 4 input currents change in this analysis, we do not expect the difference to affect the general features of the results. Thus, the Padé forms do not seem to share the symmetry found in hydrodynamics. Furthermore, this lack of symmetry seems to persist even when we choose Padé forms with positive viscosity coefficients that should correspond more closely to the hydrodynamic case.

Notice that in the unscaled data in Fig. 7 V_{bot} goes negative. Although the potential reverses sign, calculations reveal that the current flow is always from left to right, even at the bottom of the sample. In Sec. II

we showed that if the conductivity is nonlocal, then either the real-space resistivity or conductivity is negative at some point. We believe that the sign reversal in the unscaled data is simply a consequence of this fact. It should be noted that voltage reversals have in fact been measured by S. Aukkaravittayapun *et al.*[25]; however, it seems unlikely that nonlocal conductivity accounts for their results.

Before concluding this section, we note that it is possible to extend the Padé forms considered above to higher levels of approximation. Suppose one simply adds a second Padé term to the first one, for instance,

$$\hat{\sigma}_{xx}(k_x) = \Sigma_x + \frac{\Delta_1}{1+k_x^2\ell_1^2} + \frac{\Delta_2}{1+k_x^2\ell_2^2}. \tag{27}$$

There are now two length scales, and one can choose the parameters so that the conductivity has a positive viscosity and maintain the property $\sigma_{xx}(0) > \sigma_{xx}(k_x \to \infty)$. It is still possible to solve the equation $\boldsymbol{\nabla}\cdot\mathbf{j} = 0$ in a manner similar to the examples discussed above. However, one would need to differentiate the integro-differential equation four times instead of twice in order to eliminate the two integral terms. As a result, one ends up with a sixth-order equation and a lot more algebra. We have not pursued this avenue.

V. SURFACE CONSIDERATIONS

We begin this section on surface considerations with a comparison of the voltage and current distributions found using the hydrodynamic approach with those found using the Padé approach. Let us consider Case 2 from the previous section making the following parameter choices

$$\Sigma_x = \sigma_x^0 + \eta\ell^{-2}, \tag{28a}$$
$$\Delta_x^z = -\eta\ell^{-2}, \tag{28b}$$

so that the small-$\mathbf{k}$ expansion of the conductivity is

$$\sigma_{xx}(\mathbf{k}) = \sigma_x^0 + \eta k_z^2 - \eta\ell^2 k_z^4 + O(\ell^4 k_z^6). \tag{29}$$

Note that the $\ell \to 0$ limit coincides with the truncation used in the hydrodynamic approach. The fourth-order equation derived for Case 2, Eq. (20), becomes

$$\left[\ell^2\Sigma_z\partial_z^4 + \left(\eta + \ell^2\sigma_x^0\right)\partial_z^2\partial_x^2 - \sigma_x^0\partial_x^2 - \Sigma_z\partial_z^2\right] V = 0. \tag{30}$$

If the terms proportional to ℓ^2 are dropped, the equation is identical to the one studied by Huse and Majumdar [15,26]. However, notice the small parameter, ℓ^2, multiplies the highest derivative, $\partial_z^4 V$. This is the classic scenario for the development of a *boundary layer*, a small region in which V varies quite rapidly and in which $\ell^2\partial_z^4 V$ is not negligibly small.[27] Recall that our analysis of Case 2 produced two length scales given by Eq. (21). In the small-ℓ limit, ξ_+ is a small length (proportional to ℓ); while ξ_- is the length scale arising in the hydrodynamic analysis. It is tempting to conclude that one has discovered the length scale associated with Huse and Majumdar's surface currents, but a more careful analysis is in order.

Following the steps outlined in the Appendix B we can calculate $V(x,z)$ for the top geometry with an input current $I_1\sin(\pi x/L)$. ¿From it we calculate $j_x(x,z)$, the current density in the x-direction. Figure 8 shows $j_x(0,z)$ as a function of z for several values of ℓ. As ℓ decreases, the current becomes increasingly confined to the surface $z = D$, in other words, we obtain surface currents. However, they differ from those found by Huse and Majumdar[15]. For the same input current the hydrodynamic analysis predicts that the ratio of current carried in the surface to that in the bulk is

$$\frac{\text{surface current}}{\text{bulk current}} = \frac{\eta\pi^2}{\Sigma_z L^2}; \tag{31}$$

whereas Fig. 8 seems to show that *all* of the current in our solution is carried in the surface in the limit $\ell \to 0$. We confirm this result by noting that in the bulk $j_x \sim \ell$ in the small-ℓ limit, implying that we have no bulk and all surface current as $\ell \to 0$.

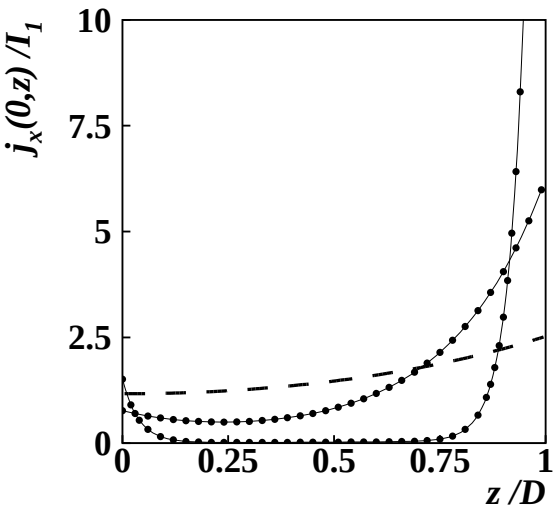

FIG. 8. The current density $j_x(0,z)$ for different values of ℓ corresponding to the Case 2 Padé conductivities, Eqs. (15b) and (28), with parameters: $\sigma_x^0 = 5$, $\eta = 5$, $\Sigma_z = 1$, $D = 1$, $L = 5$ and input current $I(x) = I_1\sin(\pi x/L)$. The dashed curve is the local curve ($\ell \to \infty$), and the other curves are for $\ell = 0.4$, and $\ell = 0.067$. The areas under the curves are equal, but as ℓ becomes smaller there is more current density at the surface.

We have examined the $\ell \to 0$ limit not because we believe it to model the real conductivity but in order to make contact with and perhaps better understand the hydrodynamic theory. Nevertheless, the outcome—that much of the current is confined to the surface—has been suggested in other contexts. If a significant fraction of the current flows in the surface, one might expect to find nonlinear behavior down to very low currents, since the current density near the surface would vary quite rapidly, leading to enormous tearing forces on the vortices. Nonlinear IV characteristics have indeed been observed in both the top geometry[28] and in $\hat{c}$-axis resistivity measurements[29]. However, our work is concerned only with the linear regime, and so we do not discuss this further.

The fact that the small-ℓ limit of Eq. (30) is identical to the corresponding hydrodynamic equation and yet the two approaches predict differing amounts of surface current suggests that it is in the treatment at the boundary (or in the effect of the boundary layer) that the two approaches differ. In the Padé calculation we considered the effect of the surface only through the boundary conditions on the current; we neglected any effect the surface might have on the nonlocal conductivity itself. One expects some surface dependence since the conductivity is determined by the superconducting order parameter, which in turn depends on the boundaries. Within the limits of their calculation, Blum and Moore[17] gave an explicit expression for the conductivity in the presence of a surface. In addition to the usual bulk conductivity their analysis yielded a term corresponding to the image of the bulk conductivity as well as "cross terms." In order to proceed with their voltage-distribution calculation analytically, the cross terms were dropped with an argument suggesting their effect was small. Subsequent work[30] has shown that the effect while small propagates farther into the bulk than was suggested in that work, indicating again the importance of treating the surface effects properly.

It may turn out that the hydrodynamic approach actually incorporates some of these surface effects. We have found that the small-ℓ limit of the Padé approach with some surface effects duplicates the hydrodynamic results. In the previous analysis, we used the conductivity in Eq. (15b) which corresponds to

$$\sigma_{xx}(\mathbf{r},\mathbf{r}') = \left[\sigma_x + \frac{\eta}{\ell^2}\right]\delta(\mathbf{r}-\mathbf{r}') - \frac{\eta G(z,z')}{\ell^2}\delta(x-x') \tag{32}$$

with

$$G(z,z') = \frac{1}{2\ell}\,\mathrm{e}^{-|z-z'|/\ell}. \tag{33}$$

Now, we modify this conductivity so that

$$G(z,z') = \frac{\cosh\left[\frac{D-|z-z'|}{\ell}\right] + \cosh\left[\frac{D-z-z'}{\ell}\right]}{2\ell\,\sinh\left[D/\ell\right]}, \tag{34}$$

which corresponds to including a series of image terms such that the nonlocal conductivity satisfies the boundary condition of its derivative vanishing on the two surfaces $z = 0$ and $z = D$. Some motivation for using this choice might come from the boundary condition the order parameter itself satisfies[17]; however, the justification here is that the results match those of the hydrodynamic approach.

Using this form, one can still solve the $\boldsymbol{\nabla}\cdot\mathbf{j} = 0$ equation in the same manner as for the conductivity of Eqs. (15). In fact, the partial differential equation one obtains as an intermediate step is the same as that obtained in Case 2 with a translationally invariant conductivity, i.e. Eq. (20). But this is to be expected since the difference lies in the boundary and not in the bulk. Applying the boundary conditions results in the following voltage distribution

$$V(x,z) = \frac{I_1 \sin\left(\frac{\pi x}{L}\right)\xi_+^2\xi_-\left(\xi_-^2-\ell^2\right)\cosh\left(\frac{z}{\xi_-}\right)}{\Sigma_z\ell^2\left(\xi_+^2-\xi_-^2\right)\sinh\left(\frac{D}{\xi_-}\right)} + \left\{\xi_- \leftrightarrow \xi_+\right\}, \tag{35}$$

which agrees with the hydrodynamic result in the $\ell \to 0$ limit. The corresponding current distribution $j_x(x,z)$

$$j_x(x,z) = \frac{I_1\frac{\pi}{L}\cos(\frac{\pi x}{L})\xi_+^2\xi_-(\eta-\sigma_x^0\xi_-^2+\sigma_x^0\ell^2)\cosh(\frac{z}{\xi_-})}{\Sigma_z\ell^2(\xi_+^2-\xi_-^2)\sinh(\frac{D}{\xi_-})} + \{\xi_- \leftrightarrow \xi_+\}, \tag{36}$$

is plotted in Fig. 9. It can be seen that once again we have surface currents in the limit $\ell \to 0$; however, this time only some of the current flows in the surface, with the rest still flowing in the bulk of the sample. In fact, the ratio of surface current to bulk current is identical to that from hydrodynamics.

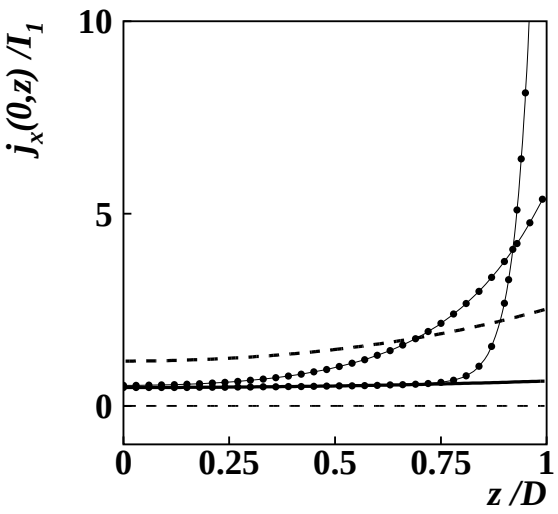

FIG. 9. The current density $j_x(0,z)$ for different values of ℓ corresponding to nontranslationally invariant conductivities of the form given by Eq. (34) with the same parameters and input current as in Fig. 8. The upper dashed curve is the local curve ($\ell \to \infty$), and the curves with •'s are for $\ell = 0.4$ and $\ell = 0.067$. The lower solid curve is the Huse and Majumdar result ($j_x(0,z) \approx 0.48\cosh(0.815z)$ for the parameters used here), which corresponds to the $\ell \to 0$ limit of our results.

This result is interesting in that it suggests that Huse and Majumdar's boundary condition may be related to surface effects in the conductivity. It is surprising that these two approaches: hydrodynamics with its translationally invariant conductivity and its slightly unusual boundary condition (associated with the discontinuity in the derivative of the electric field at the surface) and the Padé approach with a non-translationally invariant conductivity and ordinary boundary condition, can produce the same outcome.

VI. CONCLUSIONS

It is clear from the above work that the problem of nonlocal conductivity is not completely understood; however, we have made progress in developing a calculational scheme which appears to be more robust than what was available previously. Firstly, with Padé approximations, we can solve for voltage distributions having either positive or negative viscosities; whereas, hydrodynamics is limited to positive viscosities. Moreover, these approximations give the correct behavior at both high- and low-**k** and so may model the surface effects better than the hydrodynamic forms. Because measurements in the standard flux-transformer geometry are taken at the surface, an approach that deals inadequately with the surface has got to be considered suspect.

Since we now have the ability to investigate both positive and negative viscosities, we can make deductions about which sign yields the strongly nonlocal behavior seen by Safar *et al.*[3] We have found that modeling these effects seems to require positive viscosities, particularly so when the nonlocal behavior in the x direction in σ_{zz} is considered. As discussed in Sec. II, there is mounting evidence that $\hat{\sigma}_{zz}(k_z)$ may have a negative viscosity coefficient even at low temperatures, implying that the nonlocal behavior seen is not due to the dependence of $\hat{\sigma}_{zz}$ on k_z. (There are, however, other current configurations in which this is the only dependence of the conductivity probed.[17])

Finally we have discussed how the conductivity itself may be affected by surfaces and have shown that removing the translational invariance of the conductivity does not necessarily complicate the voltage-distribution calculation. In particular, we have shown that the Huse and Majumdar solution corresponds to the limit of a Padé-type solution in which the conductivity lacks translation invariance. This surprising outcome emphasizes again the importance of the surface in the problem of nonlocal conductivity and suggests that even getting the correct large-k behavior of the bulk conductivity may be insufficient if one has neglected surface effects. Fortunately, we have at least one example in which including the surface effects did not destroy the solubility of the Padé approach.

ACKNOWLEDGMENTS

The authors would like to thank T. J. Newman for very helpful discussions. S.J.P. acknowledges the support of the Engineering and Physical Science Research Council (EPSRC). T.B. acknowledges the support of EPSRC under grant GR/K53208 and of the National Science Foundation under grant DMR9312476.

APPENDIX A: ANALYSIS OF THE INFINITE-SLAB GEOMETRY

In this appendix we consider the length scales and surface effects that characterize $V_T(x,z)$ and $V_S(x,z)$, the voltage distributions in the infinite-slab geometry, by considering the pole structure of the integrals given in Eqs. (12) and (13) for a number of choices of $\hat{\sigma}_{zz}(k_x)$. The V_S integral, Eq. (13), is done by summing the residues associated with the zeros of $\cosh(\kappa D/2)$, given by $\kappa(k_x) = \pm i\pi(2m+1)/D$ with $m = 0, 1, \ldots$; the V_T integral is rather similar. For the local problem ($\hat{\sigma}_{zz}(k_x) = \Sigma_z$) these poles are evenly spaced along the imaginary axis. In fact, with δ-function-distributed input currents

$$J_T = J_0\,[\,\delta(x - 2L_c) - \delta(x + 2L_c)] \tag{A1a}$$

$$J_S = -J_0\,\delta(x + 2L_c), \tag{A1b}$$

the resulting expressions can be resummed to give

$$V_{T,S}(x,z) = \mathcal{V}\ \ln\left[\frac{\cosh\left(\dfrac{2L_c + x}{\lambda_x}\right) + \cos\left(\dfrac{\pi z}{D}\right)}{\cosh\left(\dfrac{2L_c \mp x}{\lambda_x}\right) \pm \cos\left(\dfrac{\pi z}{D}\right)}\right], \tag{A2}$$

where $\mathcal{V} = -J_0/2\pi\sqrt{\Sigma_x\Sigma_z}$ and $\lambda_x = \sqrt{\Sigma_x D^2/\pi^2\Sigma_z}$ and where the upper signs in the denominator correspond to $V_T(x,z)$ which is odd about $x = 0$ and the lower signs correspond to $V_S(x,z)$ which is odd about $z = D/2$[31].

If we consider a nonlocal part to have the hydrodynamic form $\hat{\sigma}_{zz}(k_x) = \sigma_z^0 + \eta k_x^2$, the poles are located at

$$k_x(m) = \frac{\pm i(2m+1)}{\left[\tilde{\lambda}_x^2 + \eta(2m+1)^2/\sigma_z^0\right]^{1/2}}, \tag{A3}$$

where $\tilde{\lambda}_x = \sqrt{\Sigma_x D^2/\pi^2\sigma_z^0}$. Note that the smallest pole ($m = 0$) is shifted to smaller k_x compared to the local situation ($\eta = 0$), implying a longer length scale. There is only a significant shift if the viscous length scale $\sqrt{\eta/\sigma_z^0}$ becomes comparable to the "local" length scale $\tilde{\lambda}_x$ which depends on the sample thickness D. As η increases further the viscous length dominates; we were able to resum the series in this limit, finding

$$V_S(x,z) \approx \frac{-J_0(2z-D)}{4\sqrt{\sigma_z^0\eta}} \exp\left\{-\sqrt{\frac{\sigma_z^0}{\eta}}\,|2L_c + x|\right\}. \quad \text{(A4)}$$

It would be interesting to probe the spatial dependence of V_S experimentally and extract its length scale. However, such a measurement would be difficult as it would require a sample long enough to accommodate several leads, and the voltages far from the current may become too small to be meaningful. Returning to the pole structure in the hydrodynamic case, another point to notice is that they accumulate at a finite value $\pm i\sqrt{\sigma_z^0/\eta}$. As a result $V_S(x,z)$ no longer diverges logarithmically at the contact points $(-2L_c, D)$ and $(-2L_c, 0)$. Given the δ-function input currents, this divergence is physical, and the failure of the hydrodynamic form to reproduce it is an example of how the incorrect large-$\mathbf{k}$ can affect the potential especially at the surface.

Next, let us consider $\hat{\sigma}_{zz}(k_x)$ to have a Padé form

$$\hat{\sigma}_{zz}(k_x) = \Sigma_z + \frac{\Delta_z^x}{1 + k_x^2\ell^2}. \quad \text{(A5)}$$

The small-k_x behavior of this expression is similar to the hydrodynamic example if $\Delta_z^x < 0$. However, it has twice as many poles since $\kappa(k_x) = \pm i\pi(2m+1)/D$ has twice as many solutions as in the hydrodynamic case. These poles break into two sets. For large m one set is evenly spaced and mimics the behavior in the local problem including the logarithmic divergence at the leads, while the other set accumulates at the value $\pm i\sqrt{(1+\gamma_z^x)/\ell^2}$ (where $\gamma_z^x = \Delta_z^x/\Sigma_z$) and mimics the hydrodynamic behavior in the bulk. The Padé form has clear advantages over the hydrodynamic form, but even it is not quite right since the large-k_x limit of $\hat{\sigma}_{zz}(k_x)$ should be less than $\hat{\sigma}_{zz}(0)$. To achieve that one needs something like

$$\hat{\sigma}_{zz}(k_x) = \Sigma_z\left[1 + \frac{\gamma_1}{1+k_x^2\ell^2} - \frac{\gamma_2}{(1+k_x^2\ell^2)^2}\right] \quad \text{(A6)}$$

with $\gamma_1/2 \le \gamma_2 \le \gamma_1$, which leads to three sets of poles—one like the local case and two like the hydrodynamic case. With the Padé form, Eq. (A5), one can also investigate the consequences of "negative" viscosities when $\Delta_z^x > 0$. As Δ_z^x increases, the x-axis length scale decreases and eventually a point is reached at which the poles move off the purely imaginary axis and some oscillatory behavior is superimposed on the exponential decay.

APPENDIX B: SOLUTION OF THE INTEGRO-DIFFERENTIAL EQUATION ASSOCIATED WITH THE PADÉ FORM

In this appendix we outline the solution of Case 2. For conductivities of the form given by Eq. (15b), the steady-state continuity equation $\boldsymbol{\nabla}\cdot\mathbf{j} = 0$ takes the form

$$\Sigma_x\partial_x^2 V(x,z) + \Sigma_z\partial_z^2 V(x,z) + \frac{\Delta_x^z}{2\ell}\left[\int_0^D \mathrm{e}^{-|z-z'|/\ell}\,\partial_x^2 V(x,z')\,dz'\right] = 0, \quad \text{(B1)}$$

where $\exp\{-|z-z'|/\ell\}/2\ell$ is the Fourier transform of $(1+k_z^2\ell^2)^{-1}$.

Let us now apply the following trick. Differentiate Eq. (B1) twice with respect to z, which leads to

$$\Sigma_x\partial_z^2\partial_x^2 V(x,z) + \Sigma_z\partial_z^4 V(x,z) - \frac{\Delta_x^z}{\ell^2}\partial_x^2 V(x,z) + \frac{\Delta_x^z}{2\ell^3}\left\{\int_0^D e^{-|z-z'|/\ell}\partial_x^2 V(x,z')dz'\right\} = 0, \quad \text{(B2)}$$

where we have exploited the relation

$$\frac{d^2}{dz^2}\left(\mathrm{e}^{-|z-z'|/\ell}\right) = \left[\frac{1}{\ell^2} - \frac{2}{\ell}\delta(z-z')\right]\mathrm{e}^{-|z-z'|/\ell}, \quad \text{(B3)}$$

familiar from the solution of Schrödinger's equation with a δ-function potential. We can combine Eqs. (B1) and (B2) to eliminate the integral term, giving

$$\left[\Sigma_z\partial_z^4 + \Sigma_x\partial_z^2\partial_x^2 - \frac{(\Sigma_x+\Delta_x^z)}{\ell^2}\partial_x^2 - \frac{\Sigma_z}{\ell^2}\partial_z^2\right]V = 0, \quad \text{(B4)}$$

which was given in the main body of the paper as Eq. (20).

Separating variables, $V(x,z) = X(x)\,Z(z)$, and applying the boundary condition $j_x(\pm L/2, z) = 0$ yields $X(x) = A\cos(2n\pi x/L)$ or $X(x) = B\sin[(2n+1)\pi x/L]$ for $n = 0, 1, \ldots$. When $n > 0$, the corresponding $Z(z)$ is given by

$$Z_n(z) = P_n\cosh\left(\frac{z-\frac{D}{2}}{\xi_+}\right) + Q_n\sinh\left(\frac{z-\frac{D}{2}}{\xi_+}\right) + R_n\cosh\left(\frac{z-\frac{D}{2}}{\xi_-}\right) + S_n\sinh\left(\frac{z-\frac{D}{2}}{\xi_-}\right), \quad \text{(B5)}$$

where $\xi_\pm \equiv \xi_\pm(n)$ is given by Eq. (21). For some of the algebra that follows it is convenient to choose modes that are symmetric about $z = D/2$.

It might appear that we need to apply four boundary conditions to determine the constants in $Z_n(z)$, but actually two of the constants are found by inserting the solution into the original integro-differential equation, Eq. (B1). This step yields the following two conditions

$$\frac{P_n}{R_n} = \frac{-\xi_-(\ell^2-\xi_+^2)\left[\xi_-\cosh(\frac{D}{2\xi_-})+\ell\sinh(\frac{D}{2\xi_-})\right]}{\xi_+(\ell^2-\xi_-^2)\left[\xi_+\cosh(\frac{D}{2\xi_+})+\ell\sinh(\frac{D}{2\xi_+})\right]}, \quad \text{(B6a)}$$

$$\frac{Q_n}{S_n} = \frac{-\xi_-(\ell^2-\xi_+^2)\left[\ell\cosh(\frac{D}{2\xi_-})+\xi_-\sinh(\frac{D}{2\xi_-})\right]}{\xi_+(\ell^2-\xi_-^2)\left[\ell\cosh(\frac{D}{2\xi_+})+\xi_+\sinh(\frac{D}{2\xi_+})\right]}. \quad \text{(B6b)}$$

The two remaining constants are fixed by the boundary conditions on j_z, namely

$$\begin{aligned} -\Sigma_z\partial_z V(x,D) &= I_{top}(x), \\ -\Sigma_z\partial_z V(x,0) &= I_{bot}(x). \end{aligned} \quad \text{(B7)}$$

They turn out to be fairly complicated functions of the parameters ℓ, Σ_x, Σ_z, γ_z^z, n and L, in addition to the Fourier components of $I_{top}(x)$ and $I_{bot}(x)$. Note that each $Z_n(z)$ is only a function of the corresponding Fourier component of the current. The $n=0$ part of the solution requires separate consideration; however, it is straightforward and no details are provided here.

APPENDIX C: BOSE GLASS SCALING FORMS FOR CONDUCTIVITIES

In this section we consider scaling forms for the conductivities which might be expected to hold in the presence of correlated disorder (*e.g.* columnar defects or twin boundaries). With such disorder, there is thought to be a second-order phase transition between the low-temperature Bose-glass phase and the high-temperature phase consisting of an entangled liquid of delocalized flux lines[8,9]. Near the transition the characteristic length scales $\ell_\perp$ (within the ab planes) and $\ell_\parallel$ (along the $\hat{c}$-axis) and the characteristic time scale $\tau \sim \ell_\perp^{z'}$ diverge. Nelson and Radzihovsky[32] used the scaling of the free-energy density, $f \sim 1/\ell_\parallel \ell_\perp^2$, and the vector potential, $A_\parallel \sim 1/\ell_\parallel$ and $A_\perp \sim 1/\ell_\perp$ (from gauge invariance), and the relations $\mathbf{J} = \partial f/\partial \mathbf{A}$ and $\mathbf{E} = -\partial \mathbf{A}/\partial t$ to suggest that the conductivities scale as follow

$$\begin{aligned} \sigma_\perp &\sim \ell_\parallel^{-1}\ \ell_\perp^{z'}, \\ \sigma_\parallel &\sim \ell_\parallel\ \ell_\perp^{z'-2}. \end{aligned} \quad \text{(C1)}$$

Studies of this transition[9,32] have suggested that $\ell_\parallel \sim \ell_\perp^2$ and $z' = 6.0 \pm 0.5$; we are going to use $z' = 6$.

In the Padé-form conductivities (Eqs. 15), we have a length scale ℓ, which is a $\hat{c}$-axis length scale $\ell_\parallel$ in Cases 1 and 2 and is an ab-plane length scale $\ell_\perp$ in Cases 3 and 4. Recall the conductivities in Case 1 are $\hat{\sigma}_{xx}(\mathbf{k}) = \Sigma_x$ and $\hat{\sigma}_{zz}(\mathbf{k}) = \Sigma_z + \Delta_z^z/(1+k_z^2\ell^2)$. What we want to do here is determine the dependence of the constants Σ and Δ upon ℓ. Since in this case the length scale is $\ell_\parallel$, we use $\ell_\parallel \sim \ell_\perp^2$ to eliminate the dependence upon $\ell_\perp$ and arrive at

$$\begin{aligned} \sigma_\perp^{(s)} &\sim \ell_\parallel^2, \\ \sigma_\parallel^{(s)} &\sim \ell_\parallel^3\ f(k_z\ell_\parallel), \end{aligned} \quad \text{(C2)}$$

where the superscript (s) refers to the superconducting contribution, we also include in Σ_x and Σ_z normal contributions $\sigma_x^{(n)}$ and $\sigma_z^{(n)}$ that are not affected by the scaling.

We thus obtain the following Bose-glass scaling forms:

1. $$\begin{aligned} \hat{\sigma}_{xx}(\mathbf{k}) &= \sigma_x^{(n)} + C_2\ell_\parallel^2, \\ \hat{\sigma}_{zz}(\mathbf{k}) &= \sigma_z^{(n)} + \frac{C_1\ell_\parallel^3}{1+k_z^2\ell_\parallel^2}; \end{aligned} \quad \text{(C3a)}$$

2. $$\begin{aligned} \hat{\sigma}_{xx}(\mathbf{k}) &= \sigma_x^{(n)} + \frac{C_2\ell_\parallel^2}{1+k_z^2\ell_\parallel^2}, \\ \hat{\sigma}_{zz}(\mathbf{k}) &= \sigma_z^{(n)} + C_1\ell_\parallel^3; \end{aligned} \quad \text{(C3b)}$$

3. $$\begin{aligned} \hat{\sigma}_{xx}(\mathbf{k}) &= \sigma_x^{(n)} + \frac{C_2\ell_\perp^4}{1+k_x^2\ell_\perp^2}, \\ \hat{\sigma}_{zz}(\mathbf{k}) &= \sigma_z^{(n)} + C_1\ell_\perp^6; \end{aligned} \quad \text{(C3c)}$$

4. $$\begin{aligned} \hat{\sigma}_{xx}(\mathbf{k}) &= \sigma_x^{(n)} + C_2\ell_\perp^4, \\ \hat{\sigma}_{zz}(\mathbf{k}) &= \sigma_z^{(n)} + \frac{C_1\ell_\perp^6}{1+k_x^2\ell_\perp^2}. \end{aligned} \quad \text{(C3d)}$$

It should be noted that although the constants C_1 and C_2 have no explicit dependence upon the length scales, they will be temperature-dependent. However, compared to the temperature dependence of the length scales $\ell_\perp$ and $\ell_\parallel$ near the transition, which go as powers of $|T - T_{BG}|$ (where T_{BG} is the transition temperature), it is a weak dependence. In the forms above the coefficient of the Padé term is assumed to be positive, and therefore the viscosity coefficient is negative. We can also write forms that have positive viscosity coefficients; for instance, Case 4 would be

$$\begin{aligned} \hat{\sigma}_{xx}(\mathbf{k}) &= \sigma_x^{(n)} + C_2\ell_\perp^4, \\ \hat{\sigma}_{zz}(\mathbf{k}) &= \sigma_z^{(n)} + 2C_1\ell_\perp^6 - \frac{C_1\ell_\perp^6}{1+k_x^2\ell_\perp^2}. \end{aligned} \quad \text{(C4)}$$

which is the form used to generate Fig. 6.

[1] G. Blatter, M. V. Feigel'man, V. B. Geshkenbein, A. I. Larkin and V. M. Vinokur, Rev. Mod. Phys. **66**, 1125 (1994).

[2] D. T. Fuchs, R. A. Doyle, E. Zeldov, D. Majer, W. S. Seow, R. J. Drost, T. Tamegai, S. Ooi, M. Konczykowski and P. H. Kes, Phys. Rev. B **55**, R6156 (1997).

[3] H. Safar, P. L. Gammmel, D. A. Huse, S. N. Majumdar, L. F. Schneemeyer, D. J. Bishop, D. López G. Nieva and F. de la Cruz, Phys. Rev. Lett. **72**, 1272 (1994).

[4] H. C. Montgomery, J. Appl. Phys. **42**, 2971 (1971); B. F. Logan, S. O. Rice and R. F. Wick, J. Appl. Phys. **42**, 2975 (1971).
[5] Yu. Eltsev and Ö. Rapp, Phys. Rev. Lett. **75**, 2446 (1995).
[6] D. López, E. F. Righi, G. Nieva, F. de la Cruz, W. K. Kwok, J. A. Fendrich, G. W. Crabtree and L. Paulius, Phys. Rev. B **53**, R8895 (1996); D. López, E. F. Righi, G. Nieva and F. de la Cruz, Phys. Rev. Lett. **76**, 4034 (1996).
[7] M. A. Moore, Phys. Rev. B **55**, 14136 (1997).
[8] D. R. Nelson and V. M. Vinokur, Phys. Rev. Lett. **68**, 2398 (1992); Phys. Rev. B **48**, 13060 (1993).
[9] M. Wallin and S. M. Girvin, Phys. Rev. B **47**, 14642 (1993).
[10] C. D. Keener, M. L. Trawick, S. M. Ammirata, S. E. Hebboul and J. C. Garland, Phys. Rev. B **55**, R708 (1997).
[11] R. Busch, G. Ries, H. Werthner, G. Kreiselmeyer and G. Saemann-Ischenko, Phys. Rev. Lett. **69**, 522 (1992).
[12] R. A. Doyle, W. S. Seow, Y. Wan, A. M. Campbell, T. Mochiku, K. Kadowaki and G. Wirth, Phys. Rev. Lett. **77**, 1155 (1996).
[13] G. A. Levin, J. Appl. Phys. **81**, 714 (1997).
[14] M. C. Marchetti and D. R. Nelson, Phys. Rev. B **42**, 9938 (1990); Physica C **174**, 40 (1991); M. C. Marchetti, J. Appl. Phys. **69**, 5185 (1991).
[15] D. A. Huse and S. N. Majumdar, Phys. Rev. Lett. **71**, 2473 (1993).
[16] C.-Y. Mou, R. Wortis, A. T. Dorsey and D. A. Huse, Phys. Rev. B **51** 6575 (1995).
[17] T. Blum and M. A. Moore, Phys. Rev. B **51**, 15359 (1995).
[18] R. Wortis and D. A. Huse, Phys. Rev. B **54**, 12413 (1996).
[19] J. D. Jackson, **Classical Electrodynamics** (John Wiley & Sons, New York, 1975).
[20] Y. B. Kim, C. F. Hempstead and A. R. Strnad, Phys. Rev. **139**, A1163 (1965); T. Blum and M. A. Moore, Phys. Rev. B **56** 372 (1997).
[21] S. J. Phillipson and M. A. Moore (unpublished).
[22] A. K. Kienappel and M. A. Moore (private communication).
[23] H. Safar, S. R. Foltyn, Q. X. Jia and M. P. Maley, Philos. Mag. B **74**, 647 (1996).
[24] S. Martin, A. T. Fiory, R. M. Fleming, L. F. Schneemeyer and J. V. Waszczak, Phys. Rev. Lett. **60**, 2194 (1988); G. Briceño, M. F. Crommie and A. Zettl, Phys. Rev. Lett. **66**, 2164 (1991); T. A. Friedmann, M. W. Rabin, J. Giapintzakis, J. P. Rice and D. M. Ginsberg, Phys. Rev. B **42**, 6217 (1990).
[25] S. Aukkaravittayapun, P. J. King, K. A. Benedict, Yu. I. Latyshev, I. G. Gorlova, S. Zybtsev, A. Campbell, R. A. Doyle, J. Johnson and W. S. Seow, Physica C **270**, 231 (1996).
[26] We also find the Padé boundary conditions at the sides $\pm L/2$ reduce those of Huse and Majumdar, $\left(\sigma_x^0 \partial_x - \eta \partial_x \partial_z^2\right) V(\pm L/2, z)$ in the $\ell \to 0$ limit provided we are away from $z = 0$ and $z = D$.
[27] Bender and Orszag, **Advanced Mathematical Methods for Scientists and Engineers** (McGraw-Hill, New York, 1978).
[28] D. López, G. Nieva, F. de la Cruz, H. J. Jensen and D. O'Kane, Phys. Rev. B **50**, 9684 (1994).
[29] M. C. Hellerqvist, S. Ryu, L. W. Lombardo and A. Kapitulnik, Physica C **230**, 170 (1994).
[30] S. J. Phillipson and M. A. Moore (unpublished).
[31] In situations in which the sample width is large and the terminal widths small, these expressions may offer a simplification of the *full* Montgomery analysis for extracting σ_{xx}/σ_{zz} (real or apparent). It would be distinct from the Busch procedure (ref.[11]) which approximates a series (which is slowly convergent at the top of the sample) by its first term. This being the local case, the method of images can be used to enforce the boundary conditions $\partial_x V(\pm L/2, z) = 0$. While an exact expression requires an infinite number of images, a couple should suffice to give an excellent approximation.
[32] D. R. Nelson and L. Radzihovsky, Phys. Rev. B **54**, R6845 (1996).